Oxides heterostructures for nanoelectronics

Catherine Dubourdieu, Isabelle Gélard, Olivier Salicio, Guillaume Saint-Girons, Bertrand Vilquin, Guy Hollinger

Oxides heterostructures for nanoelectronics

C. Dubourdieu*, I. Gélard and O. Salicio

Laboratoire des Matériaux et du Génie Physique (LMGP),
CNRS – Grenoble INP,
Grenoble INP-Minatec, 3 parvis L. Néel,
BP 257, 38016 Grenoble, France
Fax: +33 456529330
E-mail: Catherine.Dubourdieu@grenoble-inp.fr
E-mail: Isabelle.Gelard@grenoble-inp.fr
E-mail: Olivier.Salicio@mdm.infm.it
*Corresponding author

G. Saint-Girons, B. Vilquin and G. Hollinger

Institut des Nanotechnologies de Lyon (INL),
CNRS – Ecole Centrale de Lyon,
Ecole Centrale de Lyon, 36 avenue Guy de Collongue,
69134 Ecully, France
Fax: +33 478433593
E-mail: Guillaume.Saint-Girons@ec-lyon.fr
E-mail: Bertrand.Vilquin@ec-lyon.fr
E-mail: Guy.Hollinger@ec-lyon.fr

Abstract: We summarise in this paper the work of two groups focusing on the synthesis and characterisation of functional oxide for nanoelectronic applications. In the first section, we discuss the growth by liquid-injection MOCVD of oxides heterostructures. Interface engineering for the minimisation of silicate formation during the growth of polycrystalline $SrTiO_3$ on Si is first presented. It is realised *via* the change of reactant flow or chemical nature at the Si surface. We then report on the epitaxy on oxide substrates of manganites films and superlattices and on their magnetic and electrical properties. $La_{0.7}Sr_{0.3}MnO_3$ and $La_{0.8}MnO_{3-\delta}$ as well as multiferroic hexagonal $ReMnO_3$ manganites are considered. We show that the film thickness and related strain may be used to tune the properties. Finally, we demonstrate the growth of MgO nanowires by CVD at a moderate temperature of 600°C, using gold as a catalyst. In the second section, we discuss the growth of epitaxial oxide heterostructures by MBE. First, the direct epitaxy of $SrTiO_3$ on Si is considered. Issues and control of the $SrTiO_3$/Si interface are discussed. An abrupt interface is achieved. We show that $SrTiO_3$ on Si can be used as a buffer layer for the epitaxy of various perovskite oxides such as $LaAlO_3$ or $La_{0.7}Sr_{0.3}MnO_3$. $La_{0.7}Sr_{0.3}MnO_3$ films are ferromagnetic and metallic at room temperature. The epitaxial growth of complex oxides on Si wafers opens up the route to the integration of a wide variety of functionalities in nanoelectronics. Finally, we discuss the monolithic integration of III-V compounds such as InP on Si using epitaxial $SrTiO_3$ buffer layers for the future integration of optics on Si.

Keywords: MOCVD; MBE; epitaxy; oxide; silicon; functional; thin film; heterostructure; nanostructure; perovskite; interface; interface engineering.

Reference to this paper should be made as follows: Dubourdieu, C., Gélard, I., Salicio, O., Saint-Girons, G., Vilquin, B. and Hollinger, G. (2010) 'Oxides heterostructures for nanoelectronics', *Int. J. Nanotechnol*., Vol. 7, Nos. 4/5/6/7/8, pp.320–347.

Biographical notes: Catherine Dubourdieu received her Degree in Physics Engineering from Ecole Nationale Supérieure de Physique de Grenoble (INPG) in 1992 and her PhD Degree in Applied Physics from J. Fourier University in Grenoble in 1995. She spent 18 months as a post-doctoral fellow at Stevens Institute of Technology in Hoboken (New Jersey) and worked on the *in situ* characterisation of gas phase and film growth by optical spectroscopies during chemical vapour deposition (CVD). She joined CNRS in 1997 (at LMGP in Grenoble), where she is now Directrice de Recherche since 2007. She is the co-author of over 90 scientific papers. Her research interests are on the synthesis by CVD and on the properties of oxides heterostructures and nanostructures in relation with their micro/nanostructure (including strain) and size. She has investigated various aspects of CVD/ALD techniques: precursors benchmarking, process optimisation, plasma use for low-temperature deposition. She also works on the integration of functional oxides in micro- and nano-electronics. Since May 2009, she is a Visiting Scientist for one year at the T.J. Watson Research Center of IBM in Yorktown Heights, where she works on the integration of ferroelectric oxides on silicon.

Isabelle Gélard received her Engineering Degree from Ecole Nationale Supérieure d'Electrochimie et d'Electrométallurgie de Grenoble (INPG) in 2005 and her PhD Degree in Materials Science from Grenoble-INP in 2009. She has been working on the growth and characterisation of multiferroic heterostructures. She is now Attachée Temporaire à l'Enseignement et à la Recherche at Grenoble-INP (Phelma) where, besides teaching, she works on the physical properties of hexagonal manganite heterostructures.

Olivier Salicio received his PhD Degree in micro- and nano-electronics from the Institut National Polytechnique de Grenoble (INPG) in 2007. His PhD work has been devoted to the growth by MOCVD and to the study of $SrTiO_3$ high κ thin films on silicon for CMOS integration. He is now a post-doctoral fellow at the MDM-CNR-INFM laboratory in Agrate Brianza (Italy). He is working on the CVD of chalchogenide materials for phase change memory applications and on the ALD of lanthanide oxides for flash memory applications.

Guillaume Saint-Girons received his PhD Degree in Material Science in 2002. He joint the CNRS as a researcher in 2002, and worked during four years at the Laboratoire de Photonique et de Nanostructures (Marcoussis, France) on the growth, structural and optical properties of InAs quantum dots on GaAs and InP substrates. Since 2006, he works at the Lyon Institute of Nanotechnology (INL, Ecully France) on the epitaxial growth of crystalline oxides on silicon and on the monolithic integration of III-V semiconductors on oxides/Si. His main research interests concern the epitaxy and the structural properties of complex nanostructures and heterostructures, as well as the optical properties of III-V based light emitters. He authored or co-authored more than 50 papers in international journals, and several invited talks in international conferences.

Bertrand Vilquin graduated from University of Caen (France) and got his PhD in 2003 in the Laboratory of Professor B. Raveau. In his Doctorate Thesis, he studied the properties of graded ferroelectric films. After his doctorate,

he served as JSPS fellow in the laboratory of Professor T. Kawai (Japan) to work on *3d* transition metal oxides. In 2005, he joined the University Paris XI to design by e-beam lithography and characterise MRAM devices. In 2006, he became Associate Professor at Ecole Centrale de Lyon and is now focusing on the integration of functional oxides on silicon for novel devices.

Guy Hollinger received his Thesis Degree en 1979 from the University of Lyon. He is currently Research Director at CNRS and Director of Lyon Institute of Nanotechnology (INL). His major fields of research have been, XPS and synchrotron photoemission, surface passivation of semiconductors, epitaxial growth of strained III-V materials, new III-V thallium alloys, quantum dot heterostructures, new compliant III-V and Si pseudosubstrates, heterogeneous integration of III-V heterostructures and optoelectronic devices on silicon for optical interconnects. Since 2003, he is mainly working on epitaxial growth of oxides and on the monolithic integration on silicon. He has co-authored over 200 publications.

1 Introduction

Oxides exhibit an extremely wide variety of electrical, magnetic and optical properties, including superconductivity, piezoelectricity, ferroelectricity, pyroelectricity, ferromagnetism and multiferroicity. A review on the last developments on functional oxide can be found in a recent issue of the MRS Bulletin, devoted to the question "Whither Oxide Electronics?" [1]. Transition metal oxides, which are strongly correlated electronic systems, are particularly fascinating [2,3]. Their properties result from strong interactions between spin, charge, orbital and lattice. The several competing states give rise to complex phenomena and rich phase diagrams. Typical examples are the high-T_c superconductivity in cuprates [4,5] or the colossal magnetoresistivity (CMR) in manganites [6–8]. Due to the strong correlations in these systems, a small external perturbation leads to a huge response. Aside from the fundamental interest, the understanding and control of this complexity is of interest for applications where the diverse functionalities of these oxides could be implemented.

If single crystals are perfectly suited to study the intrinsic properties of a compound, thin films and multilayers provide new degrees of freedom to control the properties and design new one, through strain, size and interface effects. Strain imposed by a coherent epitaxy may induce a change in physical properties, such as a shift of an ordering temperature or the amplitude of a ferroelectric polarisation. Bi-axial compressively-strained epitaxial $BaTiO_3$ films exhibit a ferroelectric transition temperature nearly 500°C higher and a remanent polarisation 250% higher than bulk $BaTiO_3$ single crystals [9]. By engineering the strain and also the composition, one can take advantage of superlattice structures to tune the ferroelectric properties in a wide range [10,11].

Radically new properties can also appear from strain, size or interface effects. $SrTiO_3$, not ferroelectric as a bulk compound, becomes ferroelectric at room temperature in strained films deposited on $DyScO_3$ [12]. Size effects occur when long-range order interactions are perturbed; moreover, surfaces, which exhibit different crystalline, electronic, orbital and spin configurations, may strongly change the overall properties when they become preponderant. This is also true for interfaces, which have been the

subject of recent attention and has generated a large amount of experimental and theoretical works [13–22]. In December 2007, the journal *Science* considered the recent discoveries emerging from oxide interfaces as one of the ten breakthrough of the year 2007 [18–23]. In this emerging field, new properties arise from surfaces, electronic or orbital reconstructions. Stacking for example two insulating compounds such as $LaAlO_3$ and $SrTiO_3$ can lead to a metallic or superconducting $LaAlO_3/SrTiO_3$ interface [13–15,20]. Last but not least, interfaces in superlattices can change the nature of the coupling between competing instabilities and produce new properties. For example, superlattices combining the proper ferroelectric $PbTiO_3$ and the paraelectric $SrTiO_3$ compounds behave like a prototypical improper ferroelectric due to interface coupling based on rotational distortions [24].

In order to fully take advantage of strain and interface effects, the growth of the heterostructures must be controlled at the atomic plane level. Tremendous progresses have been achieved in this field. Pulsed-laser deposition, sputtering, molecular beam epitaxy (MBE), chemical vapour deposition (CVD) and atomic layer deposition are the most used techniques for the growth of functional oxides. As far as the integration of these oxides in devices (transistors, memories, sensors, actuators …) is concerned, few of them have now entered mainstream production. Amorphous high-dielectric permittivity (high κ) oxides, based on HfO_2, have been introduced recently in the 45-nm node for the replacement of SiO_2 as a gate oxide in CMOS field-effect transistors [25]. Ferroelectric memories based on polycrystalline films are also in production. However, many properties of interest are obtained for films epitaxially grown on oxide substrates, such as $SrTiO_3$, $LaAlO_3$ or scandates. These substrates are expensive and their size is limited. Moreover, most of potential applications are relevant if combined, on the same wafer, to Si-based CMOS functionalities. The pioneering work of McKee et al. [26], followed by other groups [27,28], has shown that the perovskite compound $SrTiO_3$ can be epitaxially grown directly on Si by MBE. This opens up the route to the integration of a wide range of oxides.

In this paper, we present the work of two groups of the Rhône-Alpes region, involved in the synthesis and characterisation of functional oxides for nanoelectronic applications.

In Section 2, we summarise selected work on such oxides grown by liquid-injection metal organic CVD. After the description of the growth technique, we first show that interface engineering on silicon can be realised by CVD through the change of the chemistry at the substrate surface. Then, the epitaxy of CMR and multiferroic manganite films and superlattices on oxide substrates and the related properties are discussed. Finally, we show that oxide nanowires can be grown by injection CVD, which opens up the route to the growth of complex oxides 1D structures.

In Section 3, we summarise selected work on functional oxides grown by MBE. After the description of the equipment, the main issues of the MBE of $SrTiO_3/Si(001)$ and $LaAlO_3/SrTiO_3/Si(001)$ are discussed, on the basis of our recent results. The applicative potential of these crystalline oxide buffers is then highlighted by discussing some examples of functional oxide integration, and by showing how the peculiarities of semiconductor/oxide heterointerfaces can be used for the monolithic growth of InP based heterostructures on $SrTiO_3/Si$.

2 Oxides nano-materials by chemical vapour deposition

2.1 Experimental: liquid-injection MOCVD

The development of innovative chemical vapour deposition (CVD) processes for the growth of complex oxides is, somehow, linked to the discovery of the high-T_c superconductor $YBa_2Cu_3O_7$ [5]. In chemical vapour deposition, the solid phase is formed on a surface from a gas phase *via* one or several chemical reactions [29]. A key issue is the generation of the gas phase, whose composition must be stable during the deposition run. Hence, the choice of the precursors as well as of the delivery scheme is of utmost importance. Since the precursors are usually liquid or solid at room temperature and atmospheric pressure, an evaporation unit is required. For Sr, Ba, or the rare-earth elements, metal-organic precursors are preferred rather than halides since they are usually volatile at a much lower temperature (≤300°C). The most used precursors so far for such elements belong to the β-diketonates family, such as tetramethyl-heptanedionate compounds (tmhd: $C_{11}H_{19}O_2$), which are solid at room temperature. These precursors can be dissolved in an appropriate solvent, like monoglyme or octane. However, the β-diketonates exhibit a very poor thermal stability at their volatilisation temperature. They tend to decompose before their complete evaporation, forming non-volatile products. Thus, if they are evaporated in classical units such as a sublimator (for powders) or a bubbler (for liquids), a drift of the vapour pressure occurs upon prolonged heating, which in turn results in a drift of the final cationic composition. This issue became very clear for the deposition of $YBa_2Cu_3O_7$, which requires a stringent control of the stoichiometry. In addition, since the evaporation temperature has to be maintained below the decomposition temperature of the precursor, very low vapour pressures were obtained.

In order to solve these issues, new evaporation schemes were developed in the early 1990s, allowing the generation of a stable gas phase from thermally-unstable and low-vapour-pressure precursors. They rely on two principles:

i the precursor is kept at room temperature under an inert gas

ii only a small amount of the precursor is introduced in the evaporator (either continuously or sequentially), where it is 'flash' volatilised.

The instantaneous volatilisation ensures that the precursor does not prematurely decompose or dissociate before evaporating. Since it is maintained at room temperature under an inert gas, its properties do not evolve during the deposition run. This delivery principle can be applied to solid [30,31] as well as liquid precursors using a syringe, a micro-pump or a liquid mass flow meter [32–36]. However, liquid- is preferred to solid-sources due to the difficulty in handling hygroscopic powders and in making homogenous mixture of different powders.

The liquid delivery scheme developed at LMGP-CNRS is based on the sequential injection of micro-amounts of liquid precursors into an evaporator where 'flash' volatilisation occurs [37–39]. The liquid is injected with an injector of the same type as those used for the fuel injection in thermal motors. It is a high-speed reliable electrovalve driven by computer. The liquid is kept in a closed vessel, pressurised under few bars of argon. The reactive species flow rate created in the evaporator depends on the electrical pulse width, which defines the volume of the droplets (typically of the

order of few μlitres), on the injection frequency of the microvalve, on the viscosity and concentration of the liquid solution and on the differential pressure between the reservoir and the evaporator. A large range of growth rates can be achieved: the minimum opening time is about 1 ms and the frequency as well as the solution dilution can be set as low as needed. On the other hand, high growth rates can be obtained (flow rates up to 50 g/min) by increasing the precursor concentration, the differential pressure and the injection frequency (the maximum working frequency is about 200 Hz). Typical growth rates for oxide deposition are 0.01–0.08 nm/injection, which allows a precise control of the thickness, down to monolayer scale. The thickness is determined by the number of injected droplets. In this delivery scheme, there is no physical contact between the liquid and the evaporator. Another advantage is the absence of dead volume, so that the growth is really stopped when the injection is stopped.

The deposition of complex oxides is realised either by injecting each precursor separately or by using a single injector fed with a liquid mixture of the different precursors. The liquid injection source is highly versatile for varying the stoichiometry or the doping of films (through the change of a liquid composition), while for PLD or sputtering techniques, a new ceramic target has to be prepared. The growth of multilayers is realised with several injectors, which are used sequentially (one for each compound to be deposited).

In a typical reactor, the deposition chamber consists of a quartz tube and a substrate holder with a hot-wall type configuration. The cylindrical hot wall is heated by rf inductive currents and the substrate holder is heated mostly by radiation. The evaporator is situated below the quartz tube. Several injectors can be connected to the evaporator. The substrate temperature, total pressure, argon and oxygen flow rates are monitored and controlled. The vapour of solvent passes in the reaction zone, which might lead to the incorporation of carbon in the films. For films deposited at 500–850°C – which is a typical temperature range for epitaxial films – XPS studies have shown that, except for a thin surface contamination layer, no carbon is detected in the films within the sensitivity of the measurement (~1%) when enough oxygen is introduced during deposition. A typical oxygen partial pressure of 2.5 Torr is used for a total pressure of 5 Torr. In order to obtain a full oxygenation of complex oxides, a post-deposition annealing is required, which is typically performed at ~800°C under 1 atm of O_2 for 15 min.

Liquid-injection CVD has been successfully used for the growth of a wide variety of oxide films and multilayers, such as high-T_c superconductors [40], high κ oxides [41–46], ferroelectrics [47–49], magnetic oxides [50–56], and multiferroics [57–60]. Epitaxial as well as polycrystalline or amorphous films can be obtained.

2.2 Interface engineering on silicon

$SrTiO_3$ has been considered as a potential gate oxide for the replacement of SiO_2 in transistors [61,62]. It has a cubic perovskite structure with $a = 3.905$ Å. The relative dielectric permittivity for the bulk compound is ~300 at room temperature. Since the band offset with the silicon conduction band is negative, it is desirable to keep a thin SiO_2 pedestal layer.

We investigated the growth and properties of $SrTiO_3$ on *n*- and *p*-type Si/SiO_2 (~1 nm) substrates. Precursors of $Sr(tmhd)_2$ and $Ti(tmhd)_2(OiPr)_2$ were used in solution

in octane or monoglyme [44] and evaporated at 250°C. The films were grown at 700°C in order to achieve a high crystalline quality and to avoid the formation of strontium carbonates. However, at such a high temperature, interface reactions may occur. A silicate layer containing Sr and Ti was evidenced by X-ray photoelectron spectroscopy. Two routes were explored in order to precisely control the growth and thickness of the interfacial silicate layer.

In the first one, the flow rate of the reactive species was modified by varying the injection period in the range of 0.1–5 s. The period, at which reactants are supplied to the surface, has a strong influence on the nucleation in the first stages of the growth. As shown in Figure 1, the silicate interfacial layer does not form when the injection period is increased (5 s). On the other hand, the silicate layer thickness strongly increases for lower periods (1 or 0.1 s). It may be related to kinetic as well as steric hindrance phenomena that does not favour $SrTiO_3$ nucleation for low injection periods.

Figure 1 TEM images of $SrTiO_3$ films grown on Si/SiO_2 substrates for three injection periods of the precursor solution: (a) 5 s, (b) 1 s and (c) 0.1 s. While no silicate layer is formed for a period of 5 s, the silicate layer thickness increases as the period decreases

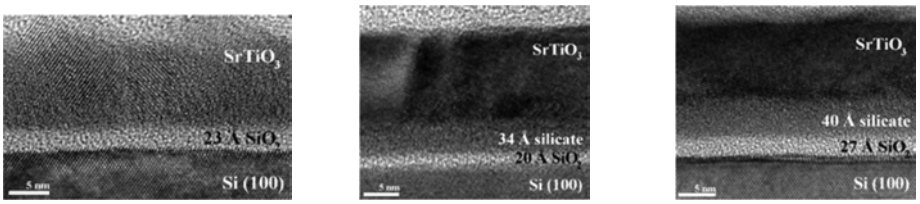

(a) (b) (c)

In the second route investigated, the precursor chemistry in the first stages of the growth was changed. We first explored the use of an hetero-metallic precursor, $Sr_2Ti_2(tmhd)_4(OiPr)_8$, instead of a mixture of two monometallic ones. With this precursor, the crystalline perovskite phase was obtained at a lower temperature of 500°C without carbonate phases (while with the mixture of precursors a minimum decomposition temperature of 600°C was needed). Moreover the film composition was constant in a wide temperature range from 550°C to 750°C. However, this hetero-metallic precursor favoured a Sr deficiency in the films (although the ratio between Sr and Ti is 1 : 1 in the precursor), which turned out to favour a thicker silicate interfacial layer. A different strategy was thus explored: first the starting SiO_2 layer was removed by a conventional HF-last treatment and then the growth was started using the $Sr(tmsa)_2$ with formula $Sr[N(SiMe_3)_2]_2$. This molecule does not contain any oxygen atoms. This precursor was injected alone in an attempt to passivate the Si surface. Such a strategy of passivation is used in MBE for the epitaxial growth of $SrTiO_3$ on Si [26,63]. After the injection of few microlitres under H_2 gas, the injection of the mixture of $Sr(tmhd)_2$ and $Ti(tmhd)_2(OiPr)_2$ precursors (under Ar and O_2 gas) was realised. XPS analyses of the Si-O peak showed that the silicate layer was significantly reduced.

These two examples show that interface engineering can be realised in CVD by changing the flow or the nature of the reactants in the first stages of the growth.

For optimised polycrystalline films, an equivalent oxide thickness (EOT) of 1.36 nm (with physical thickness of 15 nm) and a leakage current density of 10^{-2} A/cm^2 at –1 V were obtained. After taking into account the contribution from the lower interface

between $SrTiO_3$ and Si, the permittivity κ of $SrTiO_3$ was calculated to be ~70 for films of 10–15 nm. The effective permittivity of the stack is also decreased by the contribution of the upper interface with the existence of a dielectric 'dead layer'. It was shown from *ab initio* calculation that such a decrease of the permittivity at the dielectric/metallic interface is an intrinsic effect, that does exist even for perfect (no defects, no strain) interfaces [64].

While the use of $SrTiO_3$ is no more considered for future CMOS generations, this compound is investigated now as an alternative oxide for high-capacitance trench structures for memory applications.

2.3 Epitaxial functional oxides films and superlattices

2.3.1 Colossal magnetoresistive oxides

Doped-manganite perovskites $La_{1-x}A_xMnO_3$, where A is a divalent cation such as Ba, Sr or Ca, have received considerable attention in the last decade due to their spectacular properties such as the colossal magnetoresistance effect (CMR) [6–8,65–67]. They are strongly correlated electronic systems, in which spin, charge, orbital and lattice are coupled. For appropriate doping levels, these materials are ferromagnetic metals (although poor metals) with a magnetic transition at the Curie temperature T_c and a Metal-Insulator (MI) transition at the temperature T_{MI} nearby T_c. The MI transition is accompanied by the CMR effect under an applied magnetic field. $La_{0.7}Sr_{0.3}MnO_3$ has the highest Curie temperature (T_c ~ 370 K) among the manganites [68]. It is also a half metal, with a fully spin-polarised conduction band, which is highly interesting for spintronics applications. The CMR effect can also be obtained in the La-deficient manganite $La_{1-x}MnO_{3-\delta}$ ($x > 0$, $\delta > 0$) system, where the doping is realised by vacancies on the La site [69]. The ferromagnetic ordering temperature (and the related MI transition) can be adjusted by both oxygen content and La deficiency. It can reach nearly room temperature for $x \sim 0.2$ and strongly oxidised compounds [70,71], which is of interest since the CMR effect is maximum near T_c. For a given x value, the δ value will be fixed by the oxygen partial pressure–temperature conditions.

$La_{0.7}Sr_{0.3}MnO_3$ and $La_{0.8}MnO_{3-\delta}$ films were epitaxially grown on (001) $SrTiO_3$ (with $a = 3.905$ Å) and (001) $LaAlO_3$ (with $a = 3.788$ Å) substrates [70,72]. The deposition temperature was 700°C. $La(tmhd)_3$, $Sr(tmhd)_2$, and $Mn(tmhd)_3$ were used as precursors.

A cross-section TEM image of an epitaxial $La_{0.7}Sr_{0.3}MnO_3$ film on $SrTiO_3$ is shown on Figure 2(a). A high crystalline quality is observed throughout the thickness and at the interface with the substrate.

The out-of-plane lattice parameter of the films was calculated from the position of high-angle 00ℓ diffraction peaks. The films exhibit bi-axial compressive strain on $LaAlO_3$ and bi-axial tensile strain on $SrTiO_3$, which is in agreement with the lattice mismatch between bulk compound and substrate. The average c-parameter is strongly dependent on the film thickness for both types of compounds. This is illustrated in Figure 3(a) for $La_{0.8}MnO_{3-\delta}$ films grown on $LaAlO_3$. A similar behaviour was observed for $La_{0.7}Sr_{0.3}MnO_3$ films. Ultrathin films are almost pseudomorphic. Due to the post-deposition annealing, the pseudomorphic growth is not kept as thickness increases. On $LaAlO_3$, the strain relaxation leads to the progressive decrease of the c parameter as shown in Figure 3(a), and the c-value is close to the bulk value for thickness larger than

50 nm. The strain relaxation in these films was further investigated by a detailed X-ray diffraction study performed using synchrotron light source (at the National Synchrotron Light Source in Brookhaven) [73,74]. Both in-plane and out-of-plane lattice parameters were measured. Our data indicated that the films were composed of two regions, one near the substrate, which was highly constrained by the substrate lattice, and a more relaxed region away from the substrate. This two-layer model was also found in the $La_{0.7}Sr_{0.3}MnO_3$ films and reported by other groups for this manganite [75,76] as well as for charge-ordered ones [77].

Figure 2 (a) and (b): High-resolution TEM images of a $La_{0.7}Sr_{0.3}MnO_3$ film and of a $(La_{0.7}Sr_{0.3}MnO_3$ 5 u.c./$SrTiO_3$ 8 u.c.$)_{15}$ superlattice, both deposited on (001) $SrTiO_3$ and (c) $\theta/2\theta$ X-ray diffraction diagram on the 002 peak region of the same superlattice (measured at ESRF)

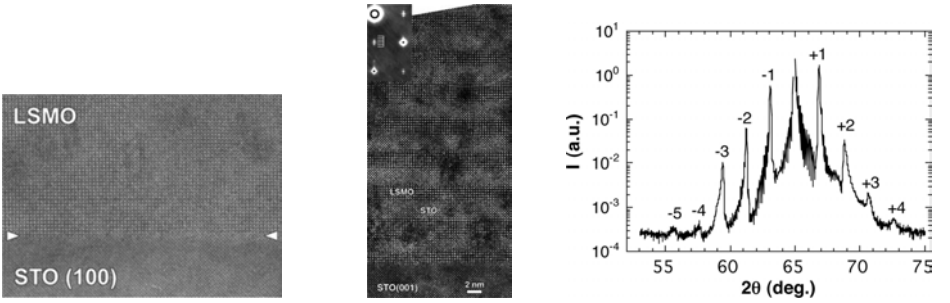

(a) (b) (c)

The magnetic properties of the films were measured using a SQUID-magnetometer. The properties of relaxed films (with thickness larger than 50 nm) are quite similar on $SrTiO_3$ and $LaAlO_3$ substrates. The films exhibit a Curie temperature T_c of 360 K and a magnetisation (at 5 K) of ~550 e.m.u./cm^3, which is comparable to the magnetisation measured in bulk samples. The resistivity (four-point probe) is ~0.06–0.07 Ω.cm and ~0.90 mΩ.cm at, respectively, 10 K and 300 K. These values are similar to those reported in the literature for such films. The metallic behaviour at room temperature makes $La_{0.7}Sr_{0.3}MnO_3$ films attractive as a bottom electrode in oxide heterostructures. $La_{0.8}MnO_{3-\delta}$ relaxed films have a T_c of ~287–295 K and a T_{MI} of ~287–295 K (see Figure 3(a) and (b)). T_c and T_{MI} depend on the value of δ. Note that the oxygen content cannot be measured precisely in thin films and is determined *a posteriori* from physical properties.

For both compounds, T_c and T_{MI} decrease with decreasing film thickness. It is shown on Figure 3(a) for $La_{0.8}MnO_{3-\delta}$ films on $LaAlO_3$. Bi-axial strains strongly influence T_c [78] but other factors are also involved such as a possible change in the crystalline structure with decreasing film thickness, magnetic disorder or defects at interfaces. In order to further investigate the size effect on T_c, we prepared $(La_{0.7}Sr_{0.3}MnO_3/SrTiO_3)_{15}$ superlattices on $SrTiO_3$ substrates, in which the thickness of $La_{0.7}Sr_{0.3}MnO_3$ was varied from 32 (~12.4 nm) to 5 unit cells (~1.9 nm) [52,79]. Figure 2(b) and (c) show a cross-section TEM image and the X-ray diffraction profile of the 002 peak region for a superlattice with 1.9 nm $La_{0.7}Sr_{0.3}MnO_3$ films. The X-ray diffraction was performed at the European Synchrotron Radiation Facility (Grenoble) on D2AM beamline. Both show that a high epitaxial crystalline quality is achieved.

The analysis of the 00ℓ diffraction lines using a program designed for the modelling of oxide superlattices [80], also confirmed the sharpness of the interfaces seen locally on the TEM images. Moreover, the coherence length is found to be equal to the total thickness (15 bilayers). A decrease of T_c was measured with decreasing manganite thickness, with a much steeper slope below ~4 nm (see Figure 31 in Haghiri and Renard [65]). Films of ~1.9 nm (5 unit cells) were still ferromagnetic. Our result is coherent with a recent study reporting that the critical thickness of such films with no ferromagnetism is ~1.2 nm (3 unit cells) [81]. We performed a Raman spectroscopy study, which evidenced a tensile-strain-induced rhombohedral (bulk-like)-to-orthorhombic phase transition when decreasing the $La_{0.7}Sr_{0.3}MnO_3$ layers from 10 nm to 3.6 nm [82]. This structural change below ~4 nm corresponds to the sharper decrease of T_c below ~4 nm. Interestingly also, our films were no more conducting for thickness of ~3.6 nm or below. A similar critical value of ~3.2 nm was reported for the metallicity in PLD $La_{0.7}Sr_{0.3}MnO_3$ films [81]. The large difference in the critical thicknesses for ferromagnetism (~1.2 nm) and metallicity (~3.2 nm) could be explained by electronic phase separation with the coexistence of ferromagnetic/metallic and nonferromagnetic/insulating regions. When the nonferromagnetic/insulating regions become larger and preponderant, no conducting path exists anymore and the film becomes insulating. Electronic phase separation in CMR manganites, which results in nanometric or micrometric spatial inhomogeneities, has been proposed theoretically and experimentally verified [83–85]. It is thought that just above the MI transition, regions of metallic phase grow within the insulating matrix and then dominate at low temperature. When the thickness is decreased, interface (substrate/film) may change competing instabilities and favour insulating regions (due to a reduction of carriers at the interface) such that the film becomes insulating and eventually no more ferromagnetic.

Figure 3 $La_{0.8}MnO_{3-\delta}$ films on $LaAlO_3$ (001) – (a): lattice parameter, T_c and T_{MI} for films with varying thickness; (b): magnetisation and resistivity and (c) effective carrier numbers and drude weight (free carriers), all as a function of temperature for a 120 nm-thick film (see online version for colours)

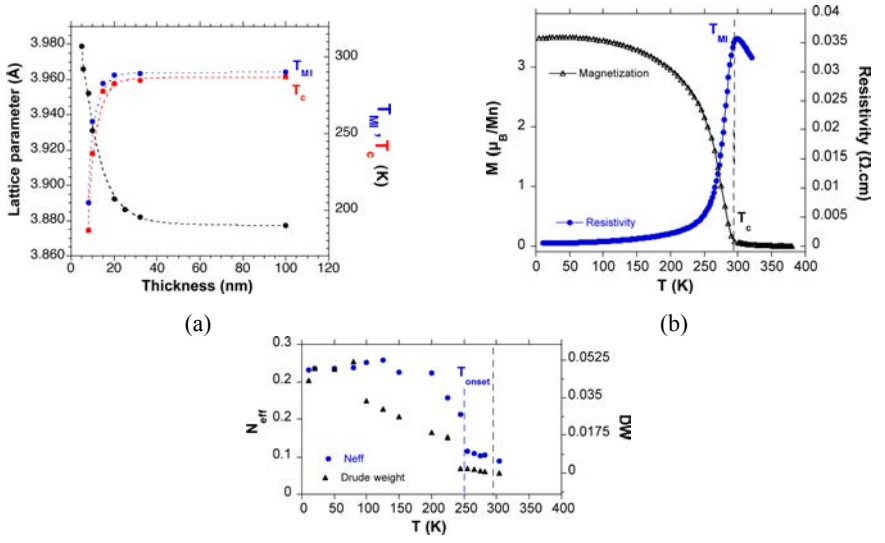

We recently evidenced by synchrotron infrared measurements such a mixed-phase behaviour in $La_{0.8}MnO_{3-\delta}$, films (thickness of 120 nm and 410 nm) grown on $LaAlO_3$ substrate [86]. Infrared reflectivity spectra were acquired over the range 100–8000 cm^{-1} and in the temperature range of 10–304 K. While the metal/insulator transition temperature T_{MI} and the magnetic ordering temperature T_c are close (~295 K), we showed that the onset of the free carrier density occurs at a significantly lower temperature (~45 K below), as shown in Figure 3(c). This indicated the presence of an insulating phase at a temperature much below T_{MI} and T_c and was consistent with the presence of insulating regions originating from local distortions, which trap the e_g conduction electrons.

In conclusion, the magnetic and transport properties of CMR compounds can be tuned in a wide range by playing with factors such as ionic radii, oxygen content, lattice strain and film thickness. Integrating epitaxial CMR oxides on Si would be of high interest for applications. This will be addressed in the second part of this paper.

2.3.2 Multiferroic hexagonal manganites

Multiferroics and more generally magneto-electric materials have recently attracted much attention [87–90]. This field has been revitalised by the extended possibilities offered by

i new probing techniques for the study of single crystals

ii the improvement of the epitaxial growth of films

iii new properties in multilayers or composites

iv progresses in *ab initio* modelling.

A multiferroic compound combines at least two ferroic orders in the same phase [87]. By extension, antiferroic orders are also included. Multiferroics, which are magnetic and ferroelectric, are of particular interest for applications [91], especially if there exists a coupling between the order parameters (magnetoelectric effect), which allows a mutual control of the properties (for example manipulating electrically a magnetisation). The fundamental understanding of the coupling between order parameters and how the local crystalline structure is involved, is still challenging. Moreover, the mechanisms involved in the possible co-existence of ferroelectricity and magnetism is highly studied in order to possibly design new materials of interest for room-temperature applications.

We have studied the properties of hexagonal $RMnO_3$ compounds. While rare-earth manganites $RMnO_3$ with R = La to Dy crystallise in a perovskite-type structure, those with R^{3+} of smaller ionic radius (Ho-Lu, Y, Sc) crystallise in a hexagonal structure of $LuMnO_3$-type with space group $P6_3cm$. Mn^{3+} ions have a coordination number of 5 (five-fold trigonal bipyramidal coordination) and R^{3+} have a coordination number of 7 (seven-fold monocapped octahedral coordination) [92]. The MnO_5 bipyramides share the corners of the trigonal basal plane O atoms. The hexagonal manganites are multiferroic compounds: they are both ferroelectric with an ordering temperature T_{FE} of ~800–1000 K and antiferromagnetic with an ordering temperature T_N of ~70–100 K. The Mn^{3+} spins order below T_N in the (a, b) basal plane, in a 120° frustrated triangular configuration. These hexagonal manganites were studied in the early 1960s by the groups of Bertaut and Koehler [92–95]. Very few works have been so far carried out on thin

films of the different rare-earth compounds, except for the study of the ferroelectric properties of $YMnO_3$ films. $YMnO_3$ has been indeed proposed as a suitable candidate for metal-ferroelectric-semiconductor structures for non-volatile memories.

Thin films of $YMnO_3$, $HoMnO_3$, $ErMnO_3$, $DyMnO_3$ and $TbMnO_3$ were grown at 850–900°C on ZrO_2:Y_2O_3 (111) and (111) Pt/TiO_2/SiO_2 /p-type (100) Si substrates [60]. $R(tmhd)_3$ and $Mn(tmhd)_3$ were used as precursors. After deposition, the samples were *in situ* annealed in 1 bar of O_2. Films of thickness 2–500 nm were prepared. Superlattices of $(YMnO_3/HoMnO_3)_{15}$ were also prepared in order to study possible enhanced magnetocapacitive effects.

All heterostructures were obtained oriented, with the *c*-axis of the hexagonal cell perpendicular to the substrate plane. This orientation is desired since it is the direction of the ferroelectric polarisation in hexagonal manganites. The films were epitaxial on YSZ with the following epitaxial relationship: $(001)_{hex.}$ $RMnO_3$//(111) YSZ and $<1–10>_{hex.}$ $RMnO_3$//<1–10> YSZ. The choice for YSZ was motivated by the fact that the (111) plane presents in-plane lattice parameters reasonably close to the in-plane parameters of the hexagonal phase of $LuMnO_3$-type and excellent coincidence of the oxygen atoms at the interface. For these reasons, it is also possible to achieve the epitaxial stabilisation of hexagonal $DyMnO_3$ or $TbMnO_3$, which normally crystallise in an orthorhombic, perovskite-type, structure (see Figure 4(a)). The formation of a coherent interface leads to the decrease of the surface energy term and thus the non-equilibrium state (hexagonal) can be stabilised by the free energy gained [57,58,96]. The Pt-buffered Si substrate was chosen as a conductive substrate for electrical characterisation. The silicon substrate underneath is of interest for future integration. However, due to the amorphous nature of SiO_2 and TiO_2 on top, the Pt is not epitaxial on Si. As a consequence, the films are not in-plane oriented. However, due to the presence of large Pt grains, a local epitaxy is achieved, as shown in Figure 4(b) for a superlattice.

The epitaxial films on YSZ exhibit in-plane tensile strain, which is in good agreement with the lattice mismatch with the substrate. The lattice mismatch is calculated as $1-\left(\sqrt{2}.a_{\text{hex}}/\sqrt{3}.a_{YSZ}\right)$, with $a_{\text{YSZ}} = 5.14$ Å. The in-plane lattice parameter a_{hex} for hexagonal $YMnO_3$, $ErMnO_3$ or $HoMnO_3$ is ~6.14 Å. Similarly to CMR manganite films, we evidenced that strain relaxation leads to a two-layer film, composed of a strained layer on the substrate and of a partially- or fully-relaxed layer on top.

The magnetic properties of the epitaxial films on YSZ were studied by neutron diffraction [97]. This technique was employed for the first time to such manganite films. An antiferromagnetic phase transition was clearly evidenced in $YMnO_3$, $ErMnO_3$, and $HoMnO_3$ films of thickness 450–500 nm by measuring 010 or 011 diffraction peaks as a function of temperature (see Figure 5). These reflections do not exist or are very weak in the crystalline structure. For $YMnO_3$ and $ErMnO_3$, the Néel temperature for the Mn^{3+} ions ordering is, respectively, 66 K and 68 K. They are about 10 K lower than in the bulk. For the $HoMnO_3$ film, a transition was observed at ~50 K. It is not yet clear whether this temperature corresponds to T_N (which normally is ~72 K) or to the reorientation temperature T_{SR}, which has been reported to be in the range of 33–50 K in bulk samples. The dependence of T_N with thickness was studied for $YMnO_3$. T_N decreases with film thickness (150 nm: ~58 K and 50 nm: ~52 K). We correlated this change to the in-plane bi-axial tensile strain, which may affect the Mn^{3+} ordering in the basal plane.

The magnetic domain size was determined from the FWHM of the diffraction peaks. It is of the order of 20–55 nm in the b^* direction of the reciprocal lattice (which is not

parallel to the *a*-axis in a hexagonal structure). These values are similar to the size of antiferromagnetic domains in $BiFeO_3$ films [98]. The domain size dependence with thickness is similar to the one reported for other ferroic compounds [99]. More data are, however, needed in order to determine the power-law dependence and a possible agreement with the model proposed by Catalan et al. [99].

Figure 4 High-resolution TEM images: (a) epitaxially-stabilised $TbMnO_3$ film on (111) YSZ substrate and (b) $(YMnO_3/HoMnO_3)_{15}$ superlattice on (111) $Pt/TiO_2/SiO_2/Si$ substrate

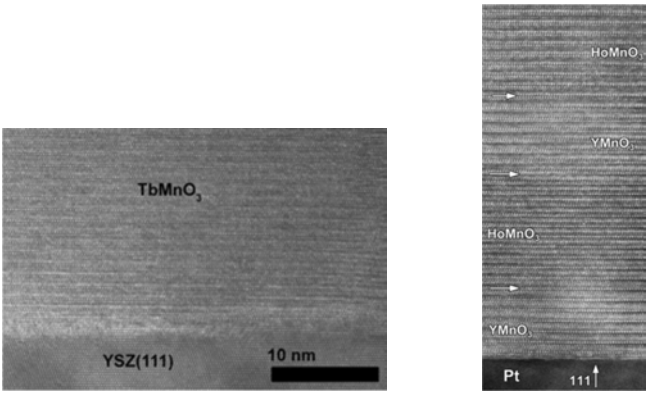

(a) (b)

Figure 5 Neutron diffraction (LLB, Saclay) performed on $YMnO_3$ (450 nm) epitaxial film: (a) 010 reflection measured at different temperatures (Gaussian fits are shown). The *x*-axis is given in reciprocal lattice units and (b) intensity of the maximum of the 010 peak as a function of temperature. Cross symbols correspond to the background level (see online version for colours)

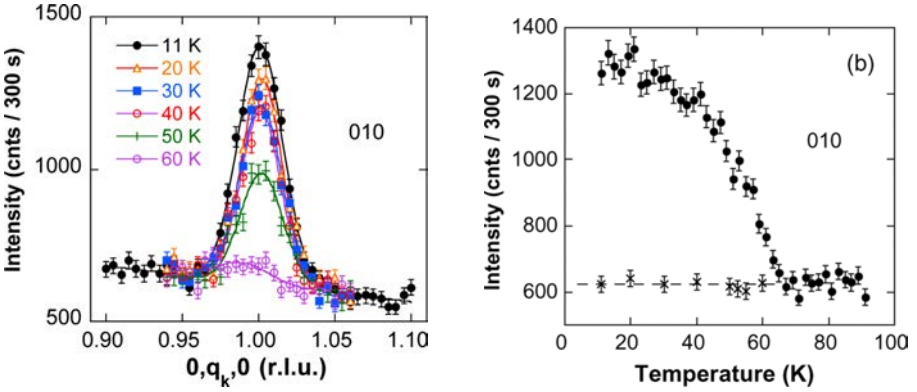

Finally, a giant magnetocapacitive effect was measured near room temperature (270 K) on a $(YMnO_3/HoMnO_3)_{15}$ superlattice prepared on Pt-buffered Si substrate [100]. The capacitance decreased by more than an order of magnitude under an applied magnetic field of 5T. This effect was attributed to extrinsic effects [101], originating from the conductive nature of the $HoMnO_3$ films. The role of possible free carriers at interfaces will be further investigated.

2.4 Oxides nanowires

The extension of the liquid injection CVD to the growth of oxide nanowires would be extremely desirable; the composition of nanowires could be for example graded or modulated at nanometre scale using several injectors. We recently demonstrated the growth of MgO nanowires by liquid-injection MOCVD at 600°C using $Mg(tmhd)_2$ as a precursor [102]. Previous studies by CVD consisted mainly in the thermal evaporation of MgB_2 [103,104] or Mg_3N_2 [105,106] powders and the condensation of MgO from the vapours (transported by a carrier gas) on a substrate placed in the furnace, next to the evaporation zone. A quite high processing temperature of 700–900°C for MgB_2 and 900–925°C for Mg_3N_2 was required. Even higher temperatures (1200°C) were needed when a mixture of MgO and carbon powder was used [107].

We used the β-diketonate $Mg(tmhd)_2$ precursor, which was dissolved in monoglyme at 0.02 mol/L. The synthesis was carried out on MgO (001) and Si (001) substrates at 600°C. The Si wafers were treated in HF acid in order to remove SiO_2. The total pressure was set at 10 Torr and the dioxygen partial pressure at 2.4 Torr. Gold was used as a catalyst. A thin gold layer of few nanometers was sputtered onto the substrates and the coated substrates were heated at 600°C for 10 min under 10 Torr. The continuous gold layer transformed into islands, whose size depended on the starting gold thickness. After the synthesis, the samples were cooled down to room temperature under 1 atm O_2. The morphology and the dimensions of the nanowires were studied by field emission scanning electron microscopy (SEM) and transmission electron microscopy (TEM), averaging data from several images. The crystalline structure of the wires was studied by X-ray diffraction and electron diffraction.

Figure 6 shows TEM and SEM images of MgO nanowires grown on MgO. It was clearly evidenced that gold acts as a catalyst. The deposition on bare MgO and Si substrates led to the formation of a continuous MgO layer. The observation of a round-shape gold nanoparticle at the tip of the wires (see Figure 6(a)), pointed out to a vapour-liquid-solid (VLS) growth mechanism [108], while the contribution from a solid/vapour mechanism could not be precluded. Both on MgO and Si substrates, TEM showed that the growth direction is along the [001]. On MgO, the wires are grown epitaxial, vertically aligned perpendicular to the substrate plane, while on Si (001), various orientations are observed. The crystallisation of the MgO cubic structure was confirmed by electron diffraction and high-resolution TEM images. The wires exhibit a square-rod shape with facets of {001} type on the sides. They have a tapered shape. The bottom 'diameter' is typically of 15–20 nm while the top diameter is of 4–5 nm. Tapering was also reported by other groups for wires grown by CVD or PVD [103,109]. The length was typically of 700 nm for 85 min deposition using an injection period of 3 s. The wires dimensions depend on several parameters, such as the starting gold catalyst thickness, the temperature, the total pressure and the oxygen partial pressure. In our conditions, a 2–3 nm gold layer thickness is optimal and leads to vertically aligned nanowires on MgO while a thicker catalyst of ~4 nm hampers the vertical growth and produces wires with a much larger difference between bottom and top dimensions and with a larger bottom diameter (~35–40 nm).

It is possible to switch the growth from vertical to horizontal by decreasing the time period at which the reactants are injected into the deposition chamber. For injection periods of 0.1–1 s, the wires grow along the substrate surface and the tapered shape is enhanced. A small injection period corresponds to a high injection rate (a period of 0.1 s

corresponds to ten precursor droplets injected per second) and, in these conditions, the diffusion along the vertical direction seems to be impeded. As previously shown in Section 2.2, the reactant flow rate is a critical parameter for the nucleation and growth at a surface.

Figure 6 MgO nanowires grown on MgO (001) substrate by injection MOCVD at 600°C: (a) High resolution TEM image and electron diffraction pattern. A gold particle at the tip of the wire is observed; (b) nanowire with Au nanoparticles along its axial axis and (c) SEM image (tilt of 30°) showing vertically-aligned MgO nanowires

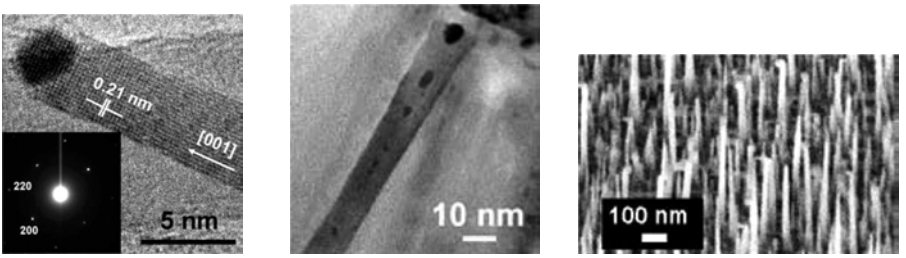

(a) (b) (c)

In most of the wires, discrete gold nanoparticles with oblong shape were observed along the central axis and with a decreasing diameter from bottom to top, as shown in Figure 6(b). Embedded gold particles in a dielectric matrix are highly interesting for optical applications. Few studies report the possibility to embed Au nanoparticles in oxide nanowires, such as SiO_2 or Ga_2O_3 [110,111]. It was proposed that the Au-in-Ga_2O_3 peapods spontaneously crystallise under phase separation induced by the formation of twin boundaries in Ga_2O_3 [111]. In our case, defects such as dislocations were observed inside the wires but did not seem to be involved in the presence of the Au particles.

In the VLS mechanism described by Wagner and Ellis [108] for the growth of Si nanowires, Si gas phase species adsorb preferentially on the liquid Au-Si droplet. Si vapour atoms enter the droplet and supersaturate it, leading to a condensation of Si at the interface between solid Si and the liquid alloy. In our case, the gaseous reactive species arriving on the droplets are $Mg(tmhd)_2$ molecules. These molecules adsorb and decompose at the liquid surface and release Mg or Mg-O gaseous species. However, the tmhd molecule and the solvent contain a large amount of C and H atoms. Although a rather high oxygen partial pressure is used, C and H species are certainly also incorporated in the liquid droplet, changing the conditions for super-saturation. Moreover, the diffusion of Mg atoms or Mg-O dimers at the catalyst droplet's surface is certainly impeded by the large amount of in- and out-diffusing species at this surface. Simultaneously, heterogeneous reactions involving the $Mg(tmhd)_2$ precursors will also take place on the substrate surface and at the sidewalls of the growing wires. Thus it is probable that the growth from the side of the wires is considerably favoured. These different facts may explain the presence of gold inside the wires. Lateral growth from the substrate surface is also consistent with the presence of facets and with the tapered shape of the wires.

The ability to grow MgO nanowires opens up the route to the growth of core/shell structures, consisting of a MgO-buffer core and a complex-oxide shell. All functionalities described in the introduction would then be accessible in 1D structures.

3 Oxides nanomaterials by molecular beam epitaxy

3.1 Experimental: molecular beam epitaxy

Molecular beam epitaxy (MBE) is a well known ultra-high vacuum growth technique, widely used for the fabrication of IV-IV and III-V materials and nanostructures. The major advantage of this growth technique relies in the possibility of controlling the deposited thickness as well as the surfaces at the atomic scale, in particular by using reflection high energy electron diffraction (RHEED). This is of particular interest for the growth of crystalline oxides on silicon, due to the fact that Si is highly reactive with respect to oxygen. The occurrence of uncontrolled interface reactions at the early stages of the growth of oxides on Si may lead to the formation of interface layers (silica, silicates, silicides) that, in general, degrade the electronic properties of the final heterostructures.

Our MBE system is a RIBER2300 reactor fully equipped for the growth of oxides. It includes Knudsen cells for the evaporation of Sr, Ti, La, and Al, as well as an electron beam gun for the direct evaporation of stoechiometric $LaAlO_3$ targets. Oxygen is introduced into the reactor *via* a pressure-regulated plasma chamber. Both atomic and molecular oxygen can be used. Element pressures are measured using a Bayard-Alpert gauge, a quartz microbalance and a mass spectrometer. The RHEED is differentially pumped in order to avoid the oxidisation of the filament. It allows *in-situ* recording of the surface roughness, in-plane lattice parameter and growth rate.

3.2 Molecular beam epitaxy for the growth of $SrTiO_3$/Si(001) and $LaAlO_3$/$SrTiO_3$/Si(001)

The main issues of the growth of $SrTiO_3$ (STO) on silicon are the control of the interface, and the control of the STO stoichiometry. The direct growth of STO on Si is impossible: even for very low oxygen partial pressures, the very low temperatures required for avoiding the formation of an amorphous silicate or SiO_2 interfacial layer lead to the growth of amorphous STO. McKee et al. [26] and IBM Zürich [63] have proposed a silicon surface passivation technique, allowing the crystalline growth of STO on Si. The Si surface, covered by its native SiO_2 layer, is exposed to Sr and heated up to approximately 700°C. This leads to the reduction of SiO_2, and to the formation of a $SrSi_2$ surface reconstruction that passivates the Si surface. Surface Sr is then oxidised under very low oxygen partial pressure (a few 10^{-8} Torr) around 400°C. Crystalline STO can then be grown in this temperature range without significant interface reaction. However, maintaining a satisfying structural quality of the oxide requires increasing the growth temperature and the oxygen partial pressure after a few monolayers. If the first few STO monolayers are not fully oxidised and stoichiometric, oxygen is liable to diffuse through STO and to react at the STO/Si interface to form an amorphous silicate interface. It has to be noted that such a process, requiring a perfect control of the interface formation and of the oxygen partial pressure in the 10^{-8} Torr range, can only be carried out by MBE.

Recent results, obtained in particular at INL [112], show that growing zero-defect STO layers on Si is a realistic objective. However, further studies and improvement of the growth process and of the control of the growth parameters have to be performed. The TEM cross-sectional view presented in Figure 7 gives an idea of the structural quality of a state-of-the art STO layer grown on Si(001).

Figure 7 TEM cross-sectional view of a STO layer grown on Si(001)

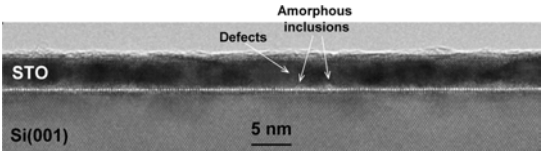

The STO layer has a flat surface, presents an abrupt interface with Si and is single crystalline. Amorphous inclusions can be seen at the interface, formed during the oxidisation of the $SrSi_2$ layer at the early stages of the growth due to an insufficient control of this crucial step. Threading defects nucleate vertically to these inclusions, separating small domains in the STO layers. These domains are slightly twisted with respect to each other, leading to an in-plane mosaicity of the layer.

Achieving zero-defect STO templates on Si(001) requires further improvements of the management of interfacial reactivity, mainly by:

- precisely controlling oxygen injection at the $SrSi_2$ oxidisation step
- improving oxygen supply during STO growth to warrant a complete oxidisation of the STO layer.

Our further studies will focus on these two points.

LAO cannot directly be grown under its crystalline form on Si(001): LAO crystallises for temperatures larger than 700°C, in growth conditions where SiO_2 and silicates are formed at the Si surface. However, STO/Si(001) templates can be used for the growth of crystalline LAO on Si(001) as shown in Figure 8 [113].

Figure 8 LAO/STO/Si(001) stack grown by MBE. An amorphous layer is formed at the STO/Si interface during the growth of LAO at 750°C, due to oxygen diffusion through the STO layer

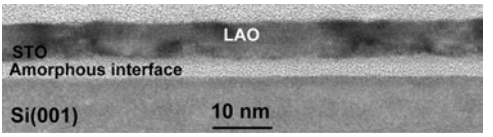

Single crystalline high-quality LAO layers can be obtained by direct electron-beam evaporation of an LAO target, at 750°C and under an oxygen partial pressure of 10^{-6} Torr. In these conditions, an amorphous silicate layer is formed at the STO/Si heterointerface due to the diffusion of oxygen through the STO layer and its reaction with silicon. This interfacial layer has no crucial impact on the structural quality of the LAO layer.

3.3 Integration of functional oxides on crystalline $SrTiO_3$/Si(001) buffers

The integration of epitaxial functional oxides on silicon opens interesting opportunities for the fabrication of novel memory, sensing, electric and optical signal processing elements. For instance, replacement of the gate dielectric by a functional oxide in the gate stack results in FET structures with increased speed (spinFET, MottFET) and increased functionality (FeFET). The possibility to combine advanced functional oxides and silicon

micro-machining opens new perspective for the development of smart sensors, eventually co-integrated with their monitoring electronics. One can then obtain robust sensors. Such applications are particularly strategic in the development of highly sensitive bio-chemical sensors operating in gaseous or liquid media. Such devices would be based on static strain-free membranes and cantilevers made of high performance piezoelectric oxide films. Optimal properties and performances are expected if the oxides are single crystalline and if a technology process can be developed to prepare the membranes (possible with epitaxial oxides on a Si substrate, which can be afterwards micro-machined).

As mentioned in the introduction, complex oxides possess as wide range of physical properties. In particular, the perovskite $La_{0.7}Sr_{0.3}MnO_3$ (LSMO) has potential use in various magnetic applications, such as magnetic memories, magnetic-field sensors, hard disc read heads, infrared devices, and micro-wave active components, to name a few, due to its CMR effect. In addition, the reasonably high electrical conductivity of LSMO and its lattice matching with other ferroelectric oxides, such as $Pb(Zr)TiO_3$ or $BaTiO_3$, make LSMO an attractive candidate as a bottom electrode material for ferroelectric perovskite heterostructures. As single-crystalline materials often exhibit superior electrical and magnetic properties, epitaxial LSMO thin films on Si are desirable for both electrical and magnetic applications.

However, there is no direct crystal lattice match between silicon and LSMO. Moreover, chemical reactions between LSMO and silicon could also occur to form interfacial phases such as silicates or silicides. Thus, appropriate buffer layers are needed in order to achieve a high epitaxial quality. Various buffer materials have been proposed [114 and references therein] but consist of complex stacks of several oxides intended to accommodate both the lattice and thermal expansion coefficient mismatches between LSMO and Si. Since high crystalline quality LSMO films can be obtained on STO substrates, a template layer of STO on Si appears ideally suited. We have thus used the STO buffer layers fabricated by MBE and presented in the previous paragraph of this paper.

LSMO films (50 nm-thick) were grown on STO (10 nm)/Si by pulsed laser deposition (PLD located at Université Paris-Sud) at a moderate temperature of 600°C to avoid silicate phase formation at the interface between silicon and STO buffer layer. The oxygen pressure during the LSMO deposition was kept at 120 mTorr and a post-annealing was performed at 300 Torr to obtain a well-oxidised ferromagnetic film. On the silicon (001) surface, the LSMO layer presents an epitaxial relationship with the STO buffer layer, i.e., a cube-on-cube growth, as shown by the X-ray diffraction measurements (Figure 9).

Rocking curve measurements give information on the spread of the c-axis distribution relatively to the substrate normal. A FWHM of about 0.5° is obtained. This value is significantly lower than the one measured for LSMO films deposited on complex buffer stacks such as $Bi_4Ti_3O_{12}/CeO_2$/yttria-stabilised-zirconia buffered Si(001) substrates (FWHM of 1.2°) [114].

The surface morphology of STO and LSMO layers was checked using AFM: STO before the LSMO growth has a rms rugosity of 0.79 nm and LSMO film a rms rugosity of 1.15 nm. Despite the difference of thermal dilatation coefficients between silicon and LSMO, the film has no crack after cooling, which confirms the good crystalline quality of the CMR layer. The R-T measurements show a MI transition temperature higher than room temperature, with a resistivity of 1 mΩ.cm

at room temperature. This value is similar to the one measured for LSMO films grown on bulk $SrTiO_3$ substrate. Finally, Magnetic Optical Kerr Effect (MOKE) characterisation performed at 300 K confirms room temperature ferromagnetism (Figure 10).

Figure 9 XRD patterns of the LSMO grown on STO buffered silicon (see online version for colours)

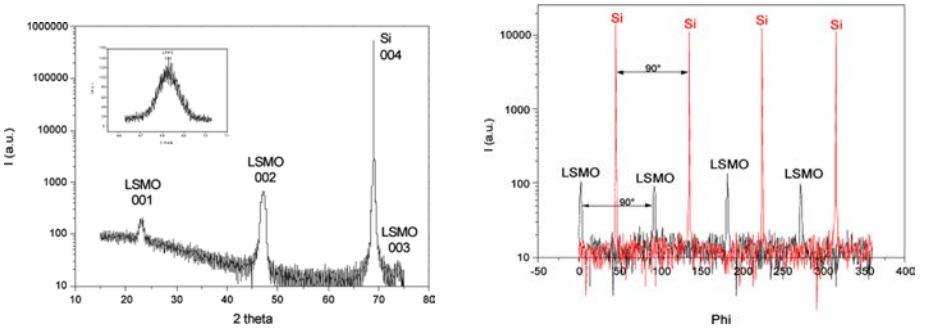

Figure 10 MOKE measurement performed at 300 K on the LSMO (see online version for colours)

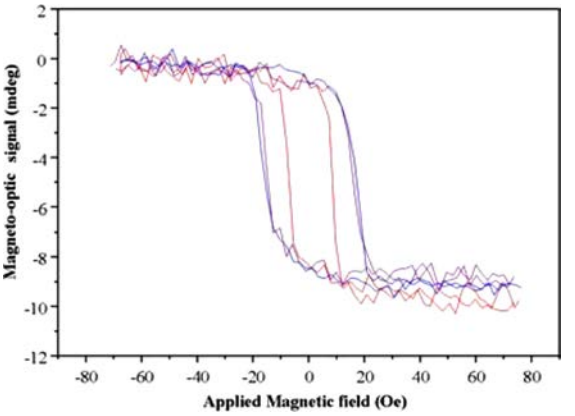

In conclusion, good quality single crystal (001)-oriented LSMO films with smooth surface, low structural defects and room temperature ferromagnetism can be grown on STO buffered-silicon, demonstrating the potential integration of high quality transition metal oxide-based devices with classical microelectronic substrates.

3.4 Monolithic integration of InP on $SrTiO_3$/Si buffers

The objective of integrating by direct epitaxy III-V or Ge on Si appears as a hot topic for further development of microelectronic systems. In particular, this could allow fabricating transistors having Ge/III-V – based high-mobility channels, and integrating III-V – based optical functionalities on Si. For that purpose, a monolithic process would offer a very interesting alternative to sticking/vignetting techniques, in terms of cost, reliability, and size that can be treated. In the field of photovoltaics, increasing the yield of solar cells (by using III-V materials) within reasonable costs (by using low cost and

large surface Si substrate and a monolithic approach) is becoming a major objective. It could also lead to the low cost fabrication of large III-V or Ge templates on Si platforms, with dimensions only limited by the size of the Si substrate.

In this context, we have recently discovered an interesting peculiarity of the InP/STO heterointerface [115,116]: when grown on a STO (001) surface, InP spontaneously takes its bulk lattice parameter as soon as the growth begins (Figure 11(a)), and does not contain any dislocation or threading defect related to any standard plastic relaxation mechanism. The large lattice mismatch (>50%) is accommodated by the formation of interfacial geometric dislocations that do no propagate in the growing layer (Figure 11(b)).

Figure 11 (a) Evolution of the 222 interatomic distance of an InP lattice grown on STO/Si(001), as deduced from *in-situ* RHEED measurements. As soon as diffraction can be detected, InP presents its bulk lattice parameter and (b) TEM cross-sectional view of an InP/STO(001) heterointerface. Inset: filtered image showing accommodation dislocations confined at the interface (see online version for colours)

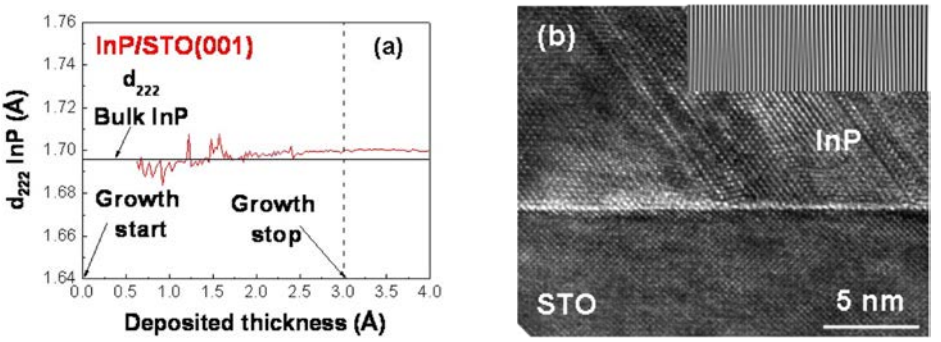

The peculiarities of the semiconductor/oxide heterointerfaces rely on their high interface energy and their high lattice mismatches: the gain in forming interfacial bonds is relatively smaller as compared to more homogeneous material systems. It is thus energetically profitable to form interfacial dislocations/dangling bonds, thus saving the cost related to elastic deformation. Good quality single crystal (001)-oriented InP layers with smooth surfaces (RMS < 0.8 nm) can be grown on STO(001). InP contains twins, the origin of which has still to be elucidated. Room temperature photoluminescence from an InAsP quantum well embedded in an InP/STO/Si(001) matrix has been observed (Figure 12). The width of the photoluminescence peak is 41 meV, equivalent to that of a quantum well grown on a bulk InP substrate.

The structural quality of InP grown on STO/Si(001) templates has to be optimised, by further improving the InP growth conditions and STO surface preparation. However, the results presented above are very promising. Very recent studies show that the GaAs/STO, InP/Gd_2O_3 [117] and Ge/$BaTiO_3$ [118] systems exhibit similar properties, demonstrating the potential of crystalline templates for the monolithic integration of III–V on Si, independently from the lattice mismatch.

Figure 12 Room-temperature photoluminescence spectrum of an InAsP quantum well embedded in an InP matrix grown on STO (001). The width of the photoluminescence peak is equivalent to that of a quantum well grown on bulk InP substrate (see online version for colours)

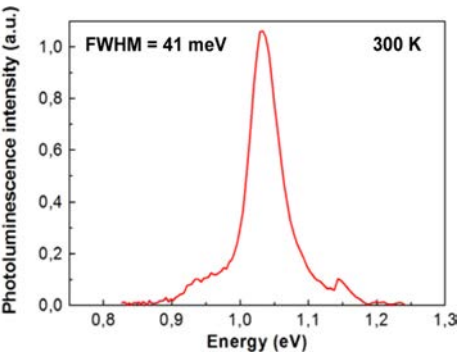

4 Conclusion

We presented our efforts towards the synthesis by CVD and MBE of functional oxides and the understanding of the resulting properties. So far, oxides, which are already on the market (such as high κ or ferroelectrics), are prepared as amorphous or polycrystalline films. However, it is clear that much more functionalities could be achieved in nanoelectronics if oxides could be integrated in the form of epitaxial films or superlattices. In this perspective, it is important to reach a high crystalline quality at the atomic scale and to understand how strain and size reduction affect the physical properties. We discussed for example how phase-transition temperatures are changed when the thickness of epitaxial CMR or multiferroic films is decreased. A high crystalline quality is achieved both by MBE and CVD on oxide substrates. However, the direct epitaxy of the perovskite $SrTiO_3$ on silicon has been achieved, so far, only by MBE. We showed that we are able to grow $SrTiO_3$ layers on Si by MBE and to use them as a template layer for the growth of $LaAlO_3$ or CMR oxide films. We also pointed out that epitaxial oxide buffer layers on Si have a high potential for the monolithic integration of III–V on Si, which would enable to combine the best of both semiconductor worlds. Finally, the ability to grow MgO nanowires is highly promising for the design of 1D complex oxide nanostructures.

Acknowledgements

This work was supported at LMGP by the French Ministère de la Recherche (ACI Nanoscience NANOINJECT), the French Ministère de l'Industrie (MEDEA+ T201, T207 and FOREMOST), the Région Rhône-Alpes (OXYDIEL project) and the European commission (NoE FAME, NoE SINANO and STREP MACoMuFi). The authors thank the following persons for their contribution to this work: Y. Lai, M. Rosina, I. Matko, P. Chaudouët, H. Roussel, G. Huot, G. Van Tendeloo, O. Lebedev, T. Tyson, E. Dooryhée and J.L. Hodeau.

The work at INL, realised on the NANOLYON platform, was partly supported by the European project PULLNANO, the French ANR projects MINOS and BOTOX, and the Region Rhône-Alpes project IMOX. The authors gratefully thank Loïc Becerra, Gang Niu, Carole Plossu, Nicolas Baboux, Philippe Regreny, Jun Cheng, Gilles Patriarche, Ludovic Largeau, Sandrine Autier-Laurent and Philippe Lecoeur for their contributions to this work.

References and Notes

1 *MRS Bulletin*, November 2008 'Wither Oxide Electronics', Vol. 33.

2 Tokura, Y. and Nagaosa, N. (2000) 'Orbital physics in transition-metal-oxides', *Science*, Vol. 288, pp.462–468.

3 Dagotto, E. (2005) 'Complexity in strongly correlated electronics systems', *Science*, Vol. 309, pp.257–262.

4 Bednorz, J.G. and Müller, K.A. (1986) 'Possible high Tc superconductivity in the Ba-La-Cu-O system', *Z. Phys. B: Condens. Matter*, Vol. 64, pp.189–193.

5 Wu, M.K., Ashburn, J.R., Torng, C.J., Hor, P.H., Meng, R.L., Gao, L., Huang, Z.J., Wang, Y.Q. and Chu, C.W. (1987) 'Superconductivity at 93 K in a new mixed-phase Y-Ba-Cu-O compound system at ambiant pressure', *Phys. Rev. Lett.*, Vol. 58, pp.908–910.

6 Ramirez, A.P. (1997) 'Colossal magnetoresistance', *J. Phys.: Condens. Matter*, Vol. 9, pp.8171–8199.

7 Coey, J.M.D. and Viret, M. (1999) 'Mixed-valence manganites', *Adv. Phys.*, Vol. 48, pp.167–293.

8 Tokura, Y. and Tomioka, Y. (1999) 'Colossal magnetoresistive manganites', *J. Magn. Magn. Mater.*, Vol. 200, pp.1–23.

9 Choi, K.J., Biegalski, M., Li, Y.L., Sharan, A., Schubert, J., Uecker, R., Reiche, P., Chen, Y.B., Pan, X.Q., Gopalan, V., Chen, L-Q., Schlom, D.G. and Eom, C.B. (2004) 'Enhancement of ferroelectricity in strained $BaTiO_3$ thin films', *Science*, Vol. 306, pp.1005–1009.

10 Rijnders, G. and Blank, D.H.A. (2005) 'Build your own superlattice', *Nature*, Vol. 433, pp.369–370.

11 Dawber, M., Stucki, N., Lichtensteiger, C., Gariglio, S., Ghosez, P. and Triscone, J-M. (2007) 'Tailoring the properties of artificially layered ferroelectric superlattices', *Adv. Mater.*, Vol. 19, pp.4153–4159.

12 Haeni, J.H., Irvin, P., Chang, W., Uecker, R., Reiche, P., Li, Y.L., Choudhury, S., Tian, W., Hawley, M.E., Craigo, B., Tagantsev, A.K., Pan, X.Q., Streiffer, S.K., Chen, L.Q., Kirchoefer, S.W., Levy, J. and Schlom, D.G. (2004) 'Room-temperature ferroelectricity in strained $SrTiO_3$', *Nature*, Vol. 430, pp.758–761.

13 Hwang, H.Y. and Ohtomo, A. (2004) 'A high-mobility electron gas at the $LaAlO_3/SrTiO_3$ heterointerface', *Nature*, Vol. 427, pp.423–426.

14 Nakagawa, N., Hwang, H.Y. and Muller, D.A. (2006) 'Why some interfaces cannot be sharp', *Nat. Mater.*, Vol. 5, pp.204–209.

15 Huijben, M., Rijnders, G., Blank, D.H.A., Bals, S., Van Aert, S., Verbeeck, J., Van Tendeloo, G., Brinkman, A. and Hilgenkamp, H. (2006) 'Electronically coupled complementary interfaces between perovskite band insulators', *Nat. Mater.*, Vol. 5, pp.556–560.

16 Fitting Kourkouris, L., Hotta, Y., Susaki, T., Hwang, H.Y. and Muller, D.A. (2006) 'Nanometer scale electronic reconstruction at the interface between $LaVO_3$ and $LaVO_4$', *Phys. Rev. Lett.*, Vol. 97, pp.256803-1–256803-4.

17 Thiel, S., Hammerl, G., Schmehl, A., Schneider, C.W. and Mannhart, J. (2006) 'Tunable quasi-two dimensional electron gases in oxide heterostructures', *Science*, Vol. 313, pp.1942–1945.

18 Ramirez, A. (2007) 'Oxide electronics emerge', *Science*, Vol. 315, pp.1377–1378.

19 Tsukazaki, A., Ohtomo, A., Kita, T., Ohno, Y., Ohno, H. and Kawasaki, M. (2007) 'Quantum Hall effect in polar oxide heterostructures', *Science*, Vol. 315, pp.1388–1391.

20 Reyren, N., Thiel, S., Caviglia, A.D., Fitting Kourkoutis, L., Hammerl, G., Richter, C., Schneider, C.W., Kopp, T., Rüetschi, A-S., Jaccard, D., Gabay, M., Muller, D.A., Triscone, J-M. and Mannhart, J. (2007) 'Superconducting interfaces between insulating oxides', *Science*, Vol. 317, No. 5842, pp.1196–1199.

21 Dagotto, E. (2007) 'When oxides meet face to face', *Science*, Vol. 318, No. 5853, pp.1076–1077.

22 Chakhalian, J., Freeland, J.W., Habermeier, H-U., Cristiani, G., Khaliullin, G., van Veenendaal, M. and Keimer, B. (2007) 'Orbital reconstruction and covalent bonding at an oxide interface', *Science*, Vol. 318, No. 5853, pp.1114–1117.

23 (2007) 'Breakthough of the year – beyond silicon?', *Science*, Vol. 318, p.1846.

24 Bousquet, E., Dawber, M., Stucki, N., Lichtensteiger, C., Hermet, P., Gariglio, S., Triscone, J-M. and Ghosez, P. (2008) 'Improper ferroelectricity in perovskite oxide artificial suerlattices', *Nature*, Vol. 452, pp.732–737.

25 Intel: www.intel.com

26 McKee, R.A., Walker, F.J. and Chisholm, M.F. (1998) 'Crystalline oxides on silicon: the first five monolayers', *Phys. Rev. Lett.*, Vol. 81, pp.3014–3017.

27 Liang, Y., Wei, Y., Hu, X.M., Yu, Z., Droopad, R., Li, H. and Moore, K. (2004) 'Heteroepitaxy of $SrTiO_3$ on vicinal Si(001): growth and kinetic effects', *J. Appl. Phys.*, Vol. 96, pp.3413–3417.

28 Delhaye, G., El Kazzi, M., Gendry, M., Hollinger, G. and Robach, Y. (2007) 'Heteroepitaxy of $SrTiO_3$ on Si and control of the interface', *Thin Solid Films*, Vol. 515, pp.6332–6336.

29 Kodas, T.T. and Hampden-Smith, M.J. (1994) *The Chemistry of Metal CVD*, VCH, Weinheim, xxiv, p.530.

30 Hiskes, R., DiCarolis, S.A., Jacowitz, R.D., Lu, Z., Feigelson, R.S., Route, R.K. and Young, J.L. (1993) 'Single source MOCVD of epitaxial thin films', *J. Cryst. Growth*, Vol. 128, pp.781–787.

31 Dubourdieu, C., Kang, S.B., Li, Y.Q., Kulesha, G. and Gallois, B. (1999) 'Solid single-source metal organic chemical vapor deposition of yttria-stabilized zirconia', *Thin Solid Films*, Vol. 339, pp.165–173.

32 Zheng, B., Eisenbraun, E.T., Liu, J. and Kaloyeros, A.E. (1992) 'Device-quality copper using chemical vapor deposition of β-diketonate source precursors in liquid solution', *Appl. Phys. Lett.*, Vol. 61, pp.2175–2177.

33 Kaul, A.R. and Seleznev, B.V. (1993) 'New principle of feeding for flash evaporation MOCVD devices', *J. Phys. IV*, Vol. 3, pp.375–378.

34 Loan, J.F. and Sullivan, J.J. (1995) 'Advanced materials delivery in CVD processing', *Semiconductor International*, Vol. 18, p.239.

35 Boer, H.J. (1996) 'Liquid-injection system based on mass flow controllers', *Solid State Technology*, Vol. 39, pp.149–152.

36 O'Brien, P., Pickett, N.L. and Otway, D.J. (2002) 'Developments in CVD delivery systems: a chemist's perspective on the chemical and physical interactions between precursors', *Chem. Vap. Deposition*, Vol. 8, pp.237–249.

37 Sénateur, J.P., Madar, M., Weiss, F., Thomas, O. and Abrutis, A. (1993) French patent FR 2707671, European Patent EP730671 (1994), US patent US 945162 (1999).

38 Sénateur, J.P., Dubourdieu, C., Weiss, F., Rosina, M. and Abrutis, A. (2000) 'Pulsed injection MOCVD of functional electronic oxides', *Adv. Mater. Opt. Electron.*, Vol. 10, pp.155–161.

39 Dubourdieu, C., Sénateur, J.P. and Weiss, F. (2002) 'MOCVD of oxide films and multilayers', in Guilloux-Viry, M. and Perrin, A. (Eds.): *Crystal Growth in Thin Solid Films: Control of Epitaxy*, ISBN 81-7736-095-7, pp.169–206.

40 Galindo, V., Sénateur, J.P., Abrutis, A., Teiserskis, A. and Weiss, F. (2000) 'High quality $YBa_2Cu_3O_{7-\delta}/PrBa_2Cu_3O_{7-\delta}$ multilayers grown by pulsed injection MOCVD', *J. Cryst. Growth*, Vol. 208, pp.357–364.

41 O'Sullivan, B., Hurley, P.K., Modreanu, M., Roussel, F., Roussel, H., Audier, M., Jimenez, C., Dubourdieu, C., Sénateur, J-P., Davies, H., Rushworth, S., Boyd, I.W., Fang, Q., Decams, J.M. and Guillon, H. (2003) 'HfO_2 films by UV assisted and thermal injection liquid source MOCVD', *Electrochemical Society Proceedings*, Vol. 2003-14, p.443.

42 Roussel, F., Roussel, H., Audier, M., Dubourdieu, C., Sénateur, J-P., Jimenez, C., Leedham, T.J., Davies, H.O., Jones, A.C., O'Sullivan, B.J., Modreanu, M., Hurley, P.K., Fang, Q. and Boyd, I.W. (2003) 'HfO_2 films obtained by injection MOCVD', *Electrochemical Society Proceedings*, Vol. 2003-08, p.907.

43 Durand, C., Dubourdieu, C., Vallée, C., Loup, V., Bonvalot, M., Renault, O., Roussel, H. and Joubert, O. (2004) 'Microstructure and electrical characterizations of yttrium oxide and yttrium silicate films deposited by pulsed liquid-injection plasma-enhanced metal-organic chemical vapor deposition', *J. Appl. Phys.*, Vol. 96, No. 3, pp.1719–1729.

44 Dubourdieu, C., Roussel, H., Jimenez, C., Audier, M., Sénateur, J.P., Lhostis, S., Auvray, L., Ducroquet, F., O'Sullivan, B.J., Hurley, P.K., Rushworth, S. and Hubert-Pfalzgraf, L. (2005) 'Pulsed liquid-injection MOCVD of high-*K* oxides for advanced semiconductor technologies', *Microelectron. Eng.*, Vol. 118, pp.105–111.

45 Durand, C., Vallée, C., Dubourdieu, C., Kahn, M., Derivaz, M., Blonkowski, S., Jalabert, D., Holliger, P., Fang, Q. and Boyd, I.W. (2006) 'Electrical property improvements of yttrium oxide-based metal-insulator-metal capacitors', *J. Vac. Sci. Technol., A*, Vol. 24, pp.459–466.

46 Dubourdieu, C., Rauwel, E., Millon, C., Chaudouët, P., Ducroquet, F., Rochat, N., Rushworth, S. and Cosnier, V. (2006) 'Growth by liquid injection MOCVD and properties of HfO_2 films for microelectronic applications', *Chem. Vap. Deposition*, Vol. 12, pp.187–192.

47 Pantou, R., Dubourdieu, C., Weiss, F., Kreisel, J., Köbernik, G. and Hässler, W. (2002) 'Effect of substitution of Ti by Zr in $BaTiO_3$ thin films grown by MOCVD', *Mater. Sci. Semicond. Process.*, Vol. 5, pp.237–241.

48 Lemée, N., Dubourdieu, C., Delabouglise, G., Sénateur, J.P. and Laroudie, F. (2002) 'Semiconductive Nb-doped $BaTiO_3$ films grown by pulsed injection MOCVD', *J. Cryst. Growth*, Vol. 235, pp.347–351.

49 Dubourdieu, C., Pantou, R., Weiss, F., Sénateur, J.P., Köbernik, G., Hässler, W., Dooryhée, E., Hodeau, J.L. and Nemoz, M. (2002) 'Structural and dielectric properties of $(BaTiO_3/SrTiO_3)_{15}$ superlattices grown by MOCVD', *Ferroelectrics*, Vol. 268, p.137.

50 Dubourdieu, C., Audier, M., Sénateur, J.P. and Pierre, J. (1999) 'Effects of the microstructure on the magneto-transport properties of manganite films grown by MOCVD', *J. Appl. Phys.*, Vol. 86, pp.6945–6955.

51 Bossak, A.A., Gorbenko, O., Yu Kaul, A.R., Graboy, I.E., Dubourdieu, C., Sénateur, J.P. and Zandbergen, H.W. (2000) 'Thin films and bulk CMR perovskite solid solution in Nd-Mn-O system', *J. Magn. Magn. Mater.*, Vol. 211, Nos. 1–3, pp.61–65.

52 Dubourdieu, C., Rosina, M., Roussel, H., Weiss, F., Sénateur, J.P. and Hodeau, J.L. (2001) 'Pulsed liquid-injection metalorganic chemical vapor deposition of $(La_{0.7}Sr_{0.3}MnO_3/SrTiO_3)_n$ superlattices', *Appl. Phys. Lett.*, Vol. 79, No. 9, pp.1246–1248.

53 Dubourdieu, C., Audier, M., Roussel, H., Sénateur, J.P. and Pierre, J. (2002) 'Crystallization and related magnetotransport properties of amorphous manganite films grown by metalorganic chemical vapor deposition', *J. Appl. Phys.*, Vol. 92, pp.379–384.

54 Steenbeck, K., Habisreuther, T., Dubourdieu, C. and Sénateur, J.P. (2002) 'Magnetic anisotropy of ferromagnetic $La_{0.7}Sr_{0.3}MnO_3$ epitaxial films deposited by MOCVD: dependence on temperature and film thickness', *Appl. Phys. Lett.*, Vol. 80, pp.3361–3363.

55 Gunnarsson, R., Ivanov, Z.G., Dubourdieu, C. and Roussel, H. (2004) 'Low-field magnetoresistance in perovskite manganites: magnetic field, temperature and current dependence', *Phys. Rev. B: Condens. Matter and Mater. Phys.*, Vol. 69, pp.054413-1–054413-6.

56 Fratila, L., Maurin, I., Dubourdieu, C. and Villégier, J.C. (2005) 'Spin-polarized quasiparticles injection in $La_{0.7}Sr_{0.3}MnO_3/SrTiO_3$/Nb heterostructure devices', *Appl. Phys. Lett.*, Vol. 86, pp.122505-1–122505-3.

57 Bossak, A., Dubourdieu, C., Sénateur, J.P., Gorbenko, O. and Yu Kaul, A.R. (2002) 'Epitaxial stabilization of hexagonal $RMnO_3$ (R=Eu, Dy) manganites', *J. Mater. Chem.*, Vol. 12, pp.800, 801.

58 Graboy, I.E., Bosak, A.A., Gorbenko, O., Yu Kaul, A.R., Dubourdieu, C., Sénateur, J.P., Svetchnikov, V.L. and Zandbergen, H.W. (2003) 'HREM study of epitaxially stabilized hexagonal rare-earth manganite films', *Chem. Mater.*, Vol. 15, pp.2632–2637.

59 Théry, J., Dubourdieu, C., Baron, T., Ternon, C., Roussel, H. and Pierre, F. (2007) 'MOCVD of $BiFeO_3$ thin films on $SrTiO_3$', *Chem. Vap. Deposition*, Vol. 13, pp.232–238.

60 Dubourdieu, C., Huot, G., Gélard, I., Roussel, H., Lebedev, O. and Van Tendeloo, G. (2007) 'Thin films and superlattices of multiferroic hexagonal rare-earth manganites', *Philos. Mag. Lett.*, Vol. 87, pp.203–210.

61 Jeon, S., Walker, F.J., Billman, C.A., McKee, R.A. and Hwang, H. (2002) 'Epitaxial $SrTiO_3$ on silicon with EOT of 5.4 Å for MOS gate dielectric applications', *International Electron Devices Meeting, Technical Digest* (Cat. N°.02CH37358), pp.955–957.

62 Jeon, S., Walker, F.J., Billman, C.A., McKee, R.A. and Hwang, H. (2003) 'Electrical characteristics of epitaxially grown $SrTiO_3$ on silicon for metal-insulator-semiconductor gate dielectric applications', *IEEE Electron Device Lett.*, Vol. 24, pp.218–220.

63 Norga, G.J., Marchiori, C., Rossel, C., Guiller, A., Locquet, J.P., Siegwart, H., Caimi, D., Fompeyrine, J., Seo, J.W. and Dieker, Ch. (2006) 'Solid phase epitaxyy of $SrTiO_3$ on (Ba,Sr)O/Si(100): the relationship between oxygen stoichiometry and interface stability', *J. Appl. Phys.*, Vol. 99, pp.84102-1–84102-7.

64 Stengel, M. and Spaldin, N. (2006) 'Origin of the dielectric dead layer in nanoscale capacitors', *Nature*, Vol. 443, pp.679–682.

65 Haghiri, A-M. and Renard, J-P. (2003) 'CMR manganites: physics, thin films and devices', *J. Phys. D: Appl. Phys.*, Vol. 36, pp.R127–R150.

66 Rao, C.N.R. and Raychaudhuri, A.K. (1998) 'Colossal magnetoresistance, charge ordering and related properties of manganese oxides', in Rao, C.N.R. and Raveau, B. (Eds.): World Scientific viii, Singapore, p.345.

67 von Helmolt, R., Wecker, J., Holzapfel, B., Schultz, L. and Samwer, K. (1993) 'Giant magnetoresistance in perovskitelike $La_{2/3}Ba_{1/3}MnO_x$ ferromagnetic films', *Phys. Rev. Lett.*, Vol. 71, pp.2331–2333.

68 Urushibara, A., Moritomo, Y., Arima, T., Asamitsu, A., Kido, G. and Tokura, Y. (1995) 'Insulator-metal transition and giant magnetoresistance in $La_{1-x}Sr_xMnO_3$', *Phys. Rev. B: Condens. Matter and Mater. Phys.*, Vol. 51, pp.14103–14109.

69 Töpfer, J. and Goodenough, J.B. (1997) 'Transport and magnetic properties of the perovskites La1-yMnO3 and LaMn1-zO3', Chem. Mater., Vol. 9, pp.1467–1474.

70 Bossak, A., Dubourdieu, C., Audier, M., Sénateur, J.P. and Pierre, J. (2004) 'Compositional effects on structure and magnetotransport properties of lacunar $La_{1-x}MnO_{3-\delta}$ ($x > 0$) films grown by MOCVD', *Appl. Phys. A*, Vol. 79, pp.1979–1984.

71 Jimenez, M., Martinez, J.L., Herrero, E., Alonso, J., Prieto, C., de Andres, A., Vallet-Regi, M., Gonzalez-Calbet, J. and Fernandez-Diaz, M.T. (1997) 'Structural and magnetoresistance study of $La_xMn_yO_{3\pm z}$', *Physica B*, Vol. 234–236, pp.708–709.

72 Bosak, A.A., Dubourdieu, C., Chaudouët, P., Sénateur, J-P. and Fournier, T. (2003) 'Magnetoresistance in step-edge junctions based on $La_{0.7}Sr_{0.3}MnO_3$ films', *J. Appl. Phys.*, Vol. 94, pp.5021–5026.

73 Qian, Q., Tyson, T.A., Dubourdieu, C., Bossak, A., Sénateur, J.P., Deleon, M., Bai, J. and Bonfait, G. (2002) 'Structural studies of annealed ultrathin $La_{0.8}MnO_3$ films', *Appl. Phys. Lett.*, Vol. 80, pp.2663–2665.

74 Qian, Q., Tyson, T.A., Dubourdieu, C., Bossak, A., Sénateur, J.P., Deleon, M., Bai, J., Bonfait, G. and Maria, J. (2002) 'Structural, magnetic and transport studies of $La_{0.8}MnO_3$ films', *J. Appl. Phys.*, Vol. 92, pp.4518–4523.

75 Ranno, L., Llobet, A., Tiron, R. and Favre-Nicolin, E. (2002) 'Strain-induced magnetic anisotropy in epitaxial manganite films', *Appl. Surf. Sci.*, Vol. 188, pp.170–175.

76 Pailloux, F., Lyonnet, R., Maurice, J-L. and Controur, J-P. (2001) 'Twinning and lattice distortions in the epitaxy of $La_{0.67}$ $Sr_{0.33}MnO_3$ thin films on (001) $SrTiO_3$', *Appl. Surf. Sci.*, Vol. 177, pp.263–267.

77 Prellier, W., Biswas, A., Rajeswari, M., Venkatesan, T. and Greene, R.L. (1999) 'Effect of substrate-induced strain on the charge-ordering transition in $Nd_{0.5}Sr_{0.5}MnO_3$', *Appl. Phys. Lett.*, Vol. 75, pp.397–399.

78 Millis, A.J., Darling, T. and Migliori, A. (1998) 'Quantifying strain dependence in 'colossal' magnetoresistance manganites', *J. Appl. Phys.*, Vol. 83, pp.1588–1591.

79 Lebedev, O.I., Verbeeck, J., Van Tendeloo, G., Dubourdieu, C., Rosina, M. and Chaudouët, P. (2003) 'Structure and properties of artificial $((La_{0.7}Sr_{0.3}MnO_3)_m/(SrTiO_3)_n)_{15}$ superlattices on (001) $SrTiO_3$', *J. Appl. Phys.*, Vol. 94, pp.7646–7656.

80 Nemoz, M., Dooryhée, E., Hodeau, J.L., Dubourdieu, C., Roussel, H. and Bayle-Guillemaud, P. (2006) 'Sensitivity of synchrotron radiation x-ray diffraction to the chemical ordering in epitaxial perovskite multilayers', *J. Appl. Phys*., Vol. 100, pp.124110-1–124110-7.

81 Huijben, M., Martin, L.W., Chu, Y-H., Holcomb, M.B., Yu, P., Rijnders, G., Blank, D.H.A. and Ramesh, R. (2008) 'Critical thickness and orbital ordering in ultrathin $La_{0.7}Sr_{0.3}MnO_3$ films', *Phys. Rev. B: Condens. Matter and Mater. Phys.*, Vol. 78, pp.094413-1–094413-7.

82 Kreisel, J., Lucazeau, G., Dubourdieu, C., Rosina, M. and Weiss, F. (2002) 'Raman scattering study of $La_{0.7}Sr_{0.3}MnO_3/SrTiO_3$ multilayers', *J. Phys.: Condens. Matter*, Vol. 14, pp.5201–5210.

83 Yunoki, S., Hu, J., Malvezzi, A.L., Moreo, A., Furukawa, N. and Dagotto, E. (1998) 'Phase sepration in electronic models for manganites', *Phys. Rev. Lett.*, Vol. 80, pp.845–848.

84 Bibes, M., Balcells, Ll., Valencia, S., Fontcuberta, J., Wojcik, M., Jedryka, E. and Nadolski, S. (2001) 'Phase separation at $La_{2/3}Ca_{1/3}MnO_3/SrTiO_3$ interfaces', *Phys. Rev. Lett.*, Vol. 87, pp.067210-1–067210-4.

85 Ahn, K.H., Lookman, T. and Bishop, A.R. (2004) 'Strain-induced metal-insulator phase coexistence in perovskite manganites', *Nature*, Vol. 428, pp.401–404.

86 Gao, P., Tyson, T.A., Liu, Z., DeLeon, M.A. and Dubourdieu, C. (2008) 'Optical evidence of mixed-phase behavior in manganite films', *Phys. Rev. B: Condens. Matter and Mater. Phys.*, Vol. 78, pp.220404-1–220404-4 (R).

87 Schmid, H. (1994) 'Multi-ferroic magnetoelectrics', *Ferroelectrics*, Vol. 162, pp.665–685.

88 Fiebig, M. (2005) 'Revival of the magnetoelectric effect', *J. Phys. D: Appl. Phys.*, Vol. 38, R123–R152.

89 Spaldin, A. and Fiebig, M. (2005) 'The renaissance of magnetoelectric multiferroics', *Science*, Vol. 309, pp.391, 392.

90 Eerenstein, W., Mathur, N.D. and Scott, J.F. (2006) 'Multiferroic and magnetoelectric materials', *Nature*, Vol. 442, pp.759–765.

91 Gajek, M., Bibes, M., Fusil, S., Bouzehouane, K., Fontcuberta, J., Barthélémy, A. and Fert, A. (2007) 'Tunnel junctions with multiferroic barriers', *Nat. Mater.*, Vol. 6, pp.296–302.

92 Yakel, H.L., Koehler, W.C., Bertaut, E.F. and Forrat, E.F. (1963) 'On the crystal structure of the manganese (III) trioxides of the heavy lanthanides and yttrium', *Acta Cryst.*, Vol. 16, pp.957–962.

93 Bertaut, E.F. and Mercier, M. (1963) 'Structure magnétique de $MnYO_3$', *Phys. Lett.*, Vol. 5, pp.27–29.

94 Bertaut, E.F., Pauthenet, R. and Mercier, M. (1963) 'Propriétés magnétiques et structures du manganite d'yttrium', *Phys. Lett.*, Vol. 7, pp.110–111.

95 Koehler, W.C., Yakel, H.L., Wollan, E.O. and Cable, J.W. (1964) 'A note on the magnetic structures of rare earth manganese oxides', *Phys. Lett.*, Vol. 9, pp.93–95.

96 Bossak, A.A. Kamenev, A.A., Graboy, I.E., Antonov, S.V., Gorbenko, O.Y., Kaul, A.R., Dubourdieu, C., Sénateur, J.P., Svechnikov, V.L., Zandbergen, H.W. and Holländer, B. (2001) 'Epitaxial phase stabilisation phenomena in rare earth manganites', *Thin Solid Films*, Vol. 400, pp.149–153.

97 Gélard, I., Dubourdieu, C., Pailhès, S., Petit, S. and Simon, Ch. (2008) 'Neutron diffraction study of hexagonal manganite $YMnO_3$, $HoMnO_3$ and $ErMnO_3$ epitaxial films', *Appl. Phys. Lett.*, Vol. 92, pp.232506-1–232506-3.

98 Béa, H., Bibes, M., Ott, F., Dupé, B., Zhu, X-H., Petit, S., Fusil, S., Deranlot, C., Bouzehouane, K. and Barthélémy, A. (2008) 'Mechanisms of exchange bias with multiferroic $BiFeO_3$ epitaxial films', *Phys. Rev. Lett.*, Vol. 100, pp.017204-1–017204-4.

99 Catalan, G., Béa, H., Fusil, S., Bibes, M., Paruch, P., Barthélémy, A. and Scott, J.F. (2008) 'Fractal dimension and size scaling of domains in thin films of multiferroic $BiFeO_3$', *Phys. Rev. Lett.*, Vol. 100, pp.027602-1–027602-4.

100 Dubourdieu, C., Huot, G. and Gélard, I. (in preparation) *Giant Magnetocapacitive Effect in an Hexagonal Manganite Superlattice*.

101 Catalan, G. (2006) 'Magnetocapacitance without magnetoelectric coupling', *Appl. Phys. Lett.*, Vol. 88, pp.102902-1–102902-3.

102 Lai, Y., Chaudouët, P., Charlot, F., Matko, I. and Dubourdieu, C. (2009) 'Magnesium oxide nanowires synthesized by pulsed liquid-injection metal organic chemical vapor deposition', *Appl. Phys. Lett.*, Vol. 94, pp.022904-1–022904-3.

103 Yin, Y., Zhang, G. and Xia, Y. (2002) 'Synthesis and characterisation of MgO nanowires through a vapor-phase precursor method', *Adv. Funct. Mater.*, Vol. 12, pp.293–298.

104 Kim, H.W. and Shim, S.H. (2006) 'Growth of MgO nanowires assisted by the annealing treatment of Au-coated substrates', *Chem. Phys. Lett.*, Vol. 422, pp.165–169.

105 Han, S., Li, C., Liu, Z., Lei, B., Zhang, D., Jin, W., Liu, X., Tang, T. and Zhou, C. (2004) 'Transition metal oxide core-shell nanowires: generic synthesis and transport properties', *Nano Lett.*, Vol. 4, pp.1241–1246.

106 Kim, G., Martens, R.L., Thompson, G.B., Kim, B.C. and Gupta, A. (2007) 'Selective area synthesis of magnesium oxide nanowires', *J. Appl. Phys.*, Vol. 102, No. 10, pp.104906-1–104906-5.

107 Yang, P. and Lieber, C.M. (1997) 'Nanostructured high-temperature superconductors: creation of strong-pinning columnar defects in nanorod/superconductor composites', *J. Mater. Res.*, Vol. 12, pp.2981–2996.

108 Wagner, R.S. and Ellis, W.C. (1964) 'Vapor-liquid-solid mechanism of single crystal growth', *Appl. Phys. Lett.*, Vol. 4, No. 5, pp.89–90.

109 Nagashima, K., Yanagida, T., Tanaka, H. and Kawai, T. (2007) 'Epitaxial growth of MgO nanowires by pulsed laser deposition', *J. Appl. Phys.*, Vol. 101, pp.124304-1–124304-4.

110 Hu, M-S., Chen, H-L., Shen, C-H., Hong, L-S., Huang, B-R., Chen, K-H. and Chen, L-C. (2006) 'Photosensitive gold-nanoparticle-embedded dielectric nanowires', *Nat. Mat.*, Vol. 5, pp.102–106.

111 Hsieh, C-H., Chou, L-J., Lin, G-R., Bando, Y. and Goldberg, D. (2008) 'Nanophotonic switch: gold-in-Ga_2O_3 peapod nanowires', *Nano Lett.*, Vol. 8, pp.3081–3085.

112 Delaye, G., Merckling, C., El-Kazzi, M., Saint-Girons, G., Gendry, M., Robach, Y., Hollinger, G., Largeau, L. and Patriarche, G. (2006) 'Structural properties of epitaxial $SrTiO_3$ thin films grown by molecular beam epitaxy on Si(001)', *J. Appl. Phys.*, Vol. 100, pp.124109-1–124109-5.

113 Merckling, C., Delaye, G., El-Kazzi, M., Gaillard, S., Rozier, Y., Rapenne, L., Chenevier, B., Marty, O., Saint-Girons, G., Gendry, M., Robach, Y. and Hollinger, G. (2007) 'Epitaxial growth of $LaAlO_3$ on Si(001) using interface engineering', *Microelectron. Reliab.*, Vol. 47, pp.540–543.

114 Méchin, L., Perna, P., Barone, C., Routoure, J-M. and Simon, Ch. (2007) '$La_{0.7}Sr_{0.3}MnO_3$ thin films on $Bi_4Ti_3O_{12}/CeO_2$/yttria-stabilised-zirconia buffered Si(001) substrates: electrical, magnetic and 1/f noise properties', *Mater. Sci. Eng., B*, Vol. 144, pp.73–77.

115 Saint-Girons, G., Priester, C., Regreny, P., Patriarche, G., Largeau, L., Favre-Nicolin, V., Xu, G., Robach, Y., Gendry, M. and Hollinger, G. (2008) 'Spontaneous compliance of the InP/$SrTiO_3$ heterointerface', *Appl. Phys. Lett.*, Vol. 92, pp.241907-1–241907-3.

116 Saint-Girons, G., Regreny, P., Cheng, J., Patriarche, G., Largeau, L., Gendry, M., Xu, G., Robach, Y., Botella, C., Grenet, G. and Hollinger, G. (2008) 'Competition between InP and In_2O_3 islands during the growth of InP on $SrTiO_3$', *J. Appl. Phys.*, Vol. 104, pp.033509-1–033509-4.

117 Saint-Girons, G., Regreny, P., Largeau, L., Patriarche, G. and Hollinger, G. (2007) 'Monolithic integration of InP based heterostructures on silicon using crystalline Gd_2O_3 buffers', *Appl. Phys. Lett.*, Vol. 91, pp.241912-1–241912-3.

118 Largeau, L., Patriarche, G., Saint-Girons, G., Delaye, G. and Hollinger, G. (2008) 'Self-assembled Ge nanocrystals on $BaTiO_3/SrTiO_3$/Si(001)', *Appl. Phys. Lett.*, Vol. 92, pp.031904-1–031904-3.